Green energy from brown seaweed: Sustainable polygeneration industrial process via fast pyrolysis of *S. Japonica* combined with the Brayton cycle

Boris Brigljević[a], Jay Liu[b,*], Hankwon Lim[a,*]

[a] *School of Energy and Chemical Engineering, Ulsan National Institute of Science and Technology (UNIST), 50 UNIST-gil, Eonyang-eup, Ulju-gun, Ulsan 44919, Republic of Korea*
[b] *Department of Chemical Engineering, Pukyong National University, 45 Yongso-ro, Nam-gu, 48513 Busan, Republic of Korea*

A B S T R A C T

Carbohydrate-rich and fast-growing seaweeds such as the *S. japonica* species are increasingly becoming the 3rd generation biomass of choice. Environmentally friendly as well as economically sound processes for biofuel production are essential if the benefits of these novel marine feedstocks are to be harnessed. This study features an experiment-based process design that combines a fluidized bed fast pyrolysis reactor system, non-intensive pretreatment, and a Bryton power cycle in an, energy-wise, nearly self-sustainable system, considerably reducing the utilization of fossil fuel-derived utilities. Complex liquid products of pyrolysis and catalytic upgrading were modeled using a specialized software ensuring strict adherence to experimental data, hence retaining a highly realistic simulation. Results of comprehensive techno-economic and market uncertainty assessments have shown a capital investment of 170 mil. USD, and a minimum selling price range of 1.534–1.852 USD/L. When compared to traditional oil and gas extraction and refining processes, the designed process yielded a 12.8-fold reduction of the total CO_2 emitted, indicating a superior process in terms of environmental sustainability.

1. Introduction

Inherent unsustainability of worldwide fossil fuel demand has led to an explosion of biofuel research in the past two decades. Potential biofuel feedstocks (organic materials) are in abundance. However, as demonstrated by the biofuel boom of 2005 [1], not all feedstocks are well-suited for large-scale production. For instance, the use of sugar and starch crops, or oil crops may lead to an increase in food prices, while land and freshwater are becoming increasingly scarce. The potential answer to this issue can be a well-integrated utilization of 2nd generation biomass as demonstrated by Özdenkçi et al. [2] as well as co-pyrolysis of biomass with synthetic waste materials (plastics) [3]. However where lignocellulosic biomass is available in abundance 3rd generation biofuel feedstocks such as aquatic biomass (i.e., micro- and macro-algae) have been intensively studied for biofuel production [4–6]. There are several advantages in using aquatic biomass. Land is not required for their cultivation, while at the same time the marine cultivation area is considerably larger. Aquatic biomass is also able to fixate carbon dioxide (CO_2) better with a greater photosynthetic efficiency of ~6–8% as opposed to terrestrial biomass which has a photosynthetic efficiency of ~1.8–2.2% [7]. However, to be considered for an industrial biofuel production process, compositional disadvantages

(such as high moisture and mineral contents) must be taken into account before utilizing aquatic biomass as a feedstock [8].

The brown macroalga or seaweed: *S. japonica* is commonly found in southeast Asia. *S. japonica* has several advantages over terrestrial biomass sources. It can be harvested four to six times per year owing to its rapid growth, and it has a superior CO_2 fixation ability of up to ~36.7 tons per ha. [7,9,10]. Besides that, *S. japonica* also has a considerably higher carbon uptake and energy density than other macroalgae [7]. Depending on geographical location and seasonal variation it contains large carbohydrate contents varying from 36 to 60 wt% [8,11,12]. Global production of *S. japonica* in 2010 was 5.14 million tons, while its harvesting infrastructure is well-developed and highly productive [13]. Therefore, this macroalga is quite well suited for cultivation as a source of biomass for biofuel production.

Numerous researchers have shown that macroalgae behave similarly to terrestrial feedstocks under pyrolysis process in terms of product phase distribution and composition variation with regards to process conditions (temperature, pressure, heating rate, retention time, etc.) [14–18]. The main obstacle for the macroalgae pyrolysis is their high mineral content which lowers the heating value of the products and poses a potential risk towards equipment and may damage it due to slag formation. Nevertheless, this challenge can be overcome via pre-
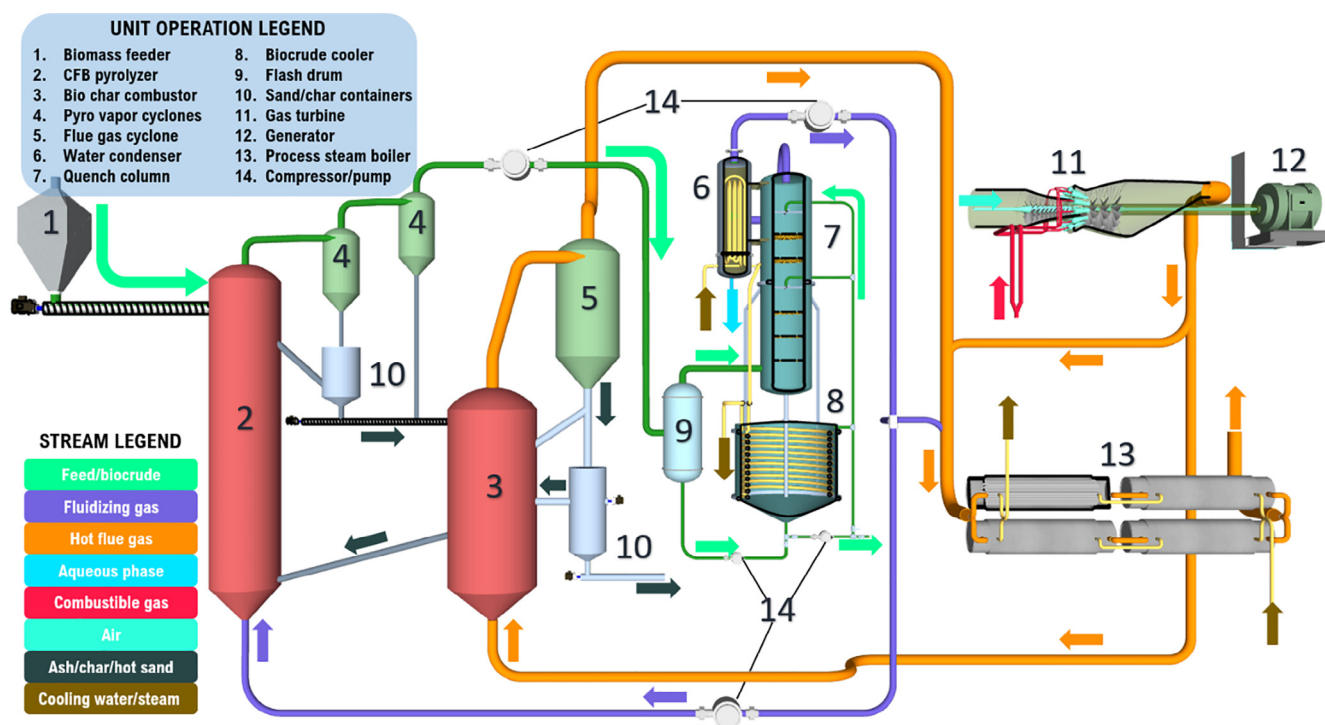

Fig. 1. Process design concept combining circulating fluidized bed fast pyrolysis with gas turbine for the production of upgraded biocrude fuel, heat and power.

treatment, commonly either by water washing and/or acid washing [19,20]. Another proven biomass pretreatment method in terms of reduction of mineral content as well as improving the pyrolysis process in general is the combined water washing and torrefaction liquid pretreatment as reported by Chen et al. [21,22]. In fact in the most recent study Cen et al. [23] has shown that using aqueous phase pyrolysis product for rice straw pretreatment yields superior results compared to both water and dilute acid wash, which could very well be one of the solutions for seaweed biomass as well. It is an accepted practice that in biofuel production research experimental studies should be followed and supported by industrial-scale techno-economic, energy and environmental feasibility studies. So far, such studies have been performed for terrestrial biomass: sugarcane [24–26], corn stover [27,28], lignocellulosic biomass [29–33]. For instance, Huang et al. [26] evaluated a lipid-cane based biodiesel process on a 1.6 million MT of feedstock per year scale with a biodiesel yield of 60.1 L/MT of lipid cane feedstock (20 wt% lipid). Total capital investment (TCI) and biodiesel cost varied with the lipid content in the feedstock from 158.5 million USD to 199 million USD and 0.86 $/L to 0.59 $/L. Corn stover pyrolysis was evaluated by Wright et al. who reported diesel and naphtha range fuels produced at 2000 dry ton per day of feedstock [34]. Hydrogen production and purchase scenarios were investigated, and TCIs reported at 287 million USD and 200 million USD, with selling prices of 0.82 USD/L and 0.56 USD/L respectively. Works detailing large-scale feasibility of aquatic biomass-based biofuel production have been reported mostly for microalgae [35–40]. Most recently Kaur et al. [41] have performed a study utilizing waste aquatic weed L. minor in which it was determined the potential advantages of utilization of this biomass compared to lignocellulosic biomass, as well as the advantages of combining biomass production with waste remediation. Although a promising research the author has concluded underlining the importance of a detailed techno-economic study including modeling and simulation for the precise determination of the process economics and scale-up feasibility. Macroalgae or seaweeds remain a relatively novel source of feedstock in thermochemical conversion processes. While they present informative techno economical assessments in terms of TCI and product selling prices, such studies are rarely based solely on

experimental data, do not provide realistic price range variations, nor quantify the environmental benefits in terms of CO_2 reduction.

This study presents a comprehensive process design, simulation, techno-economical assessment and environmental comparison with a crude oil refinery. The process is comparable in scale to biochemical conversion-based biorefineries utilizing the same feedstock as reported by Fasahati et al. [42–44], and thermochemical based biorefineries based on the reactor concept utilizing lignocellulosic feedstocks as reported by Jones and Wright [45,46]. Process design relies predominately on published data for fluidized bed pyrolysis of brown seaweed and catalytic upgrading of the pyrolysis oils to upgraded biocrude fuel. Specialized complex mixture modeling method [47] for organic liquids in biofuel production processes (such as biocrudes) was used with strict adherence to experimental data. Thus, a rigorous and realistic process simulation was ensured. Furthermore, the process design itself presents a novelty in terms of a gas turbine integration into an industrial circulating fluidized bed pyrolysis system for superior heat integration and energy efficiency. Recently Nguyen et al. [48] has performed comprehensive techno-economic analyses of several biomass catalytic hydropyrolysis processes utilizing a combination of process simulation, sensitivity and market uncertainty analyses, while Zhang et al. has analyzed economic feasibility of an industrial scale integrated thermochemical conversion process [49]. In a similar fashion, detailed techno-economic assessment and market uncertainty analyses of this novel process resulted in product selling prices ranges from minimum (minimum product selling price) to several other cases of process profitability. The selling prices are compared with traditional crude oil derived diesel fuel and the price difference is quantitatively explained through a simplistic environmental comparison.

2. Process design concept

The process designed entailed a fast pyrolysis-based biofuel production which utilizes *S. japonica* as a feedstock and produces sustainable upgraded biocrude fuel, heat and power on an industrial scale of 2.66 million wet tons per year (assuming 85 wt% moisture content). Essence of the concept of the seaweed polygeneration process design is

depicted in Fig. 1. Water-washed seaweed is fed (1) to the top of the CFB pyrolizer (2). Gaseous phase (pyrolysis vapors, gaseous products, and fluidizing gasses) is cleaned from solid particles (bio-char and sand) in a series of cyclones (4) before it is transported in a flash drum (9) where the part of pyrolysis products which have condensed is separated from the vapors. The heavy organics are fully condensed in a quench column (7) by contacting a spray of recirculated biocrude from the biocrude cooler tank (8). The water condenser (6) separates the aqueous phase from the light gasses which are partly recirculated to the CFB pyrolizer where they act as a fluidizing medium. Bio-char and sand are transported to the bio-char combustor (3) where the char is burned heating up the sand for pyrolysis. The heat and power demand of the process is supplied by the gas turbine (11), which utilizes combustible gasses and light organics from the refining process as fuel. Part of the hot flue gasses from the gas turbine is sent to the bio-char combustor (3), where it acts as a fluidizing gas and an oxidizer. After combustion flue gas from the bio-char combustor is separated from fly ash and sand particles in a cyclone (5) before it joins the remainder of the flue gas stream from the gas turbine and provides heat in a process steam boiler (13). Based on this core concept a full-scale biofuel production process was designed consisting of 6 major process areas (Fig. 2).

2.1. Pretreatment (A100)

The pretreatment section (Figure S1) starts with reducing the size of wet raw seaweed (85 wt% water content) in a hammer mill with into a pumpable mesh. The mesh is then passed through a screen filter removing the bulk of seawater and reducing the water content of seaweed to 30 wt%. The seaweed is then mixed with freshwater in the mass ratio of 1.4:1 in the favor of water, the majority of which is recycled from the process. About 7 ton/h of new freshwater is required for washing. Seaweed and freshwater mixture are passed through a series of rotary vacuum filters where the ash content is reduced by 8–10 wt% and water content is reduced to 30 wt%. The seaweed is then preheated in a series of two heat exchangers (HX) utilizing the heat from the gas turbine heat transfer fluid and hot pyrolysis gases in the first and the second HX, respectively. Final drying operation is performed by a convective rotary

dryer which utilizes part of the hot flue gasses coming from A200 as a heat source. The flue gas temperature is previously increased as the flammable compounds evolved in A200 are burned in a gas combustor. The seaweed exits the pretreatment area with the water content of 5 wt % and ash content of 26.6 wt% (reduced from 33.6 wt%).

2.2. Circulating fluidized bed (CFB) pyrolysis (A200)

This process section (Figure S2) covers primary thermochemical conversion (pyrolysis) utilizing circulating fluidized bed (CFB) reactor system. The industrial-scale CFB pyrolysis reactor and accompanying system was conceptualized and scaled from a system described by Dutta et al. [50]. Dry seaweed at around 100 °C is transported to a fluidized bed pyrolizer where it makes direct contact with the heat transfer material. The heat transfer material is fine olivine sand (Mg_2SiO_4-Fe_2SiO_4) which enters the pyrolizer at around 470 °C. The fluidizing gas originates from the A300 section and contains mostly CO_2 and CO (70 mol %) and light hydrocarbons. The mass ratios of olivine sand and fluidizing gas compared to feed are 8.5 and 1 respectively. The seaweed is pyrolyzed at an average temperature of 400 °C, and the pyrolysis vapors, along with fluidizing gas are separated from bio-char and olivine mixture in a series of cyclones. Bio-char and olivine mixture are transported to a fluidized bed combustor where hot gas turbine exhaust is introduced and the remaining combustible species in the bio-char are combusted. Olivine sand and fly ash from bio-char are separated from hot flue gases in a cyclone. Since olivine sand is heavier than fly ash it is assumed that most of the sand will be separated from the ash without the need for a more sophisticated solid–solid separators (i.e. fine mesh; electrostatic precipitator). Nevertheless, to account for a non-perfect separation, an olivine sand replenish is assumed at 0.5 ton/h. The hot pyrolysis vapors and fluidizing gas mixture is passed through a heat exchanger described in section A100 where they are cooled down to 120 °C. Condensed pyrolysis liquid is pumped to A300, and the remaining pyrolysis vapors and fluidizing gas are compressed to A300.

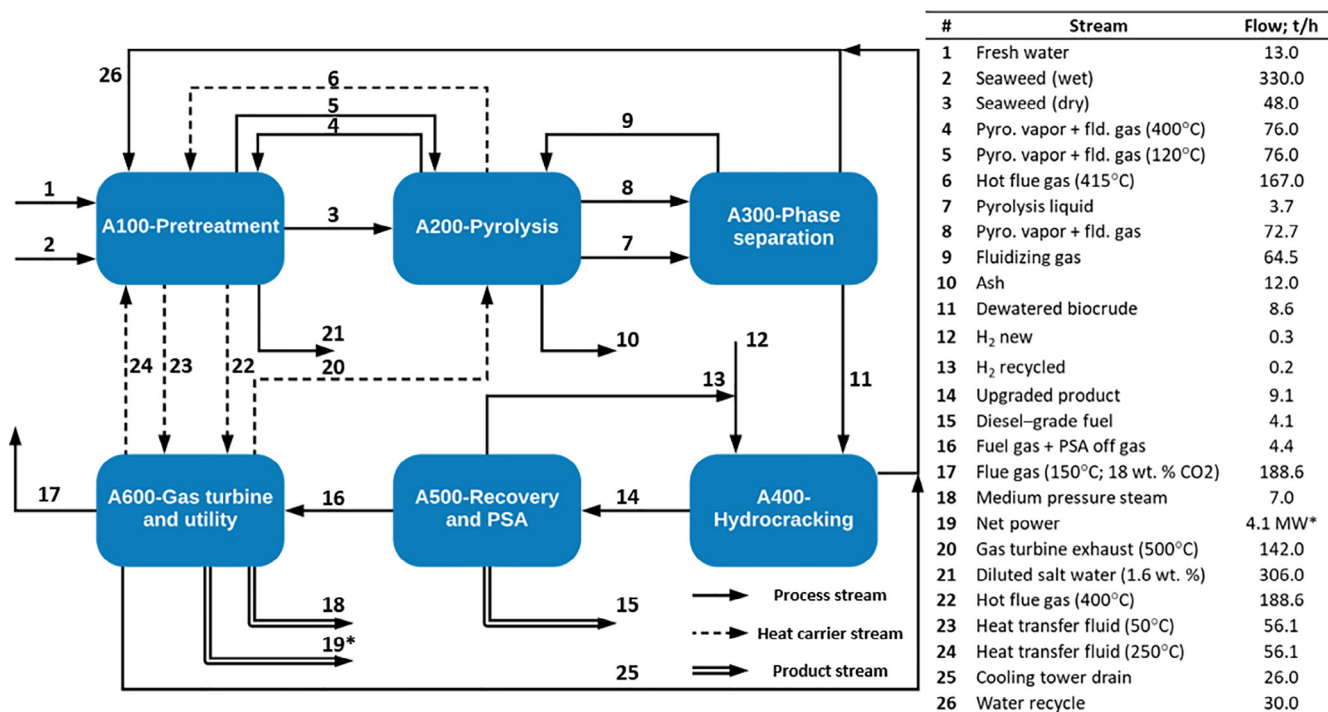| #	Stream	Flow; t/h
1	Fresh water	13.0
2	Seaweed (wet)	330.0
3	Seaweed (dry)	48.0
4	Pyro. vapor + fld. gas (400°C)	76.0
5	Pyro. vapor + fld. gas (120°C)	76.0
6	Hot flue gas (415°C)	167.0
7	Pyrolysis liquid	3.7
8	Pyro. vapor + fld. gas	72.7
9	Fluidizing gas	64.5
10	Ash	12.0
11	Dewatered biocrude	8.6
12	H_2 new	0.3
13	H_2 recycled	0.2
14	Upgraded product	9.1
15	Diesel–grade fuel	4.1
16	Fuel gas + PSA off gas	4.4
17	Flue gas (150°C; 18 wt. % CO2)	188.6
18	Medium pressure steam	7.0
19	Net power	4.1 MW*
20	Gas turbine exhaust (500°C)	142.0
21	Diluted salt water (1.6 wt. %)	306.0
22	Hot flue gas (400°C)	188.6
23	Heat transfer fluid (50°C)	56.1
24	Heat transfer fluid (250°C)	56.1
25	Cooling tower drain	26.0
26	Water recycle	30.0

Fig. 2. Block flow diagram (BFD) of the complete process indicating main process areas and material streams with a corresponding stream flow summary.
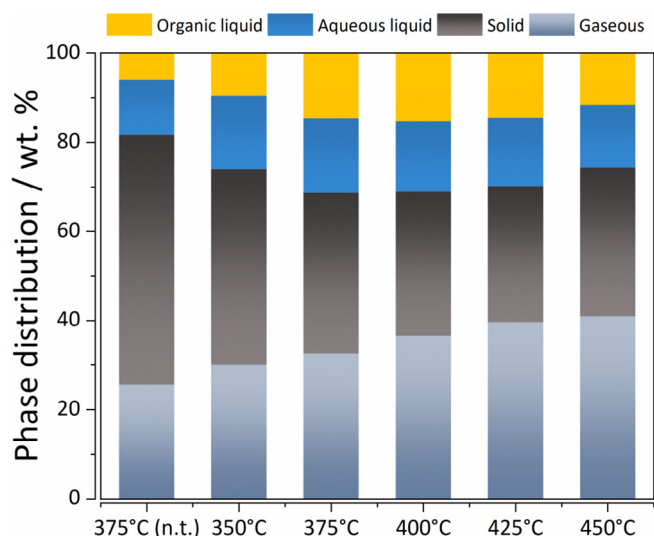
Fig. 3. Fluidized bed pyrolysis of water-washed *S. japonica* seaweed product phase distribution; (n.t. -not water-washed). Data from Choi et al. [19].

2.3. Phase separation (A300)

In the phase separation section (Figure S3) the remaining pyrolysis vapors are cooled down from 120 °C to 90 °C preheating the feed water for steam generation, and from 90 °C to 70 °C using cooling water. Flash drum separates light gasses from condensed liquids which are routed to a distillation column. The distillation column feed mixes with the organic phase recycle stream and enters the distillation column with 35 wt% water content. The column has five stages (feed enters above stage 4) with partial vapor–liquid condenser and a standard kettle reboiler. The column bottoms are mixed with pyrolysis liquids from A200 and are pumped to area A400 as dewatered biocrude (water content 6 wt%). The vapor–liquid distillate is degassed in a flash drum and the gasses are mixed with the gas stream from the first degassing process. Residual organic phase from the liquids is decanted and recycled to the distillation column, whereas aqueous stream is mixed with water streams from A600 and A400 and recycled to A100 for water washing.

2.4. Hydrocracking (A400), recovery and PSA (A500)

The biocrude is pumped to 100 bar and mixed with pressurized hydrogen (100 bar). The stream is heated to a reaction temperature of 300 °C using the reactor output stream which is at 350 °C due to the exothermal reaction. The reactor is a pressurized vessel at 100 bars, in which catalytic hydrogenation occurs (Figure S4). The product stream is depressurized to 25 bar and vapors are removed from liquids in a flash drum. The vapors are mixed with recirculated liquid and brought into recovery distillation column. The bottoms are mixed with liquid product and the mixture is cooled down to 25 °C. Three phase separator decants the aqueous phase from the product which is mixed with other aqueous phases in A300. Gasses are mixed with PSA off-gasses and sent to A600 to be used as a fuel source. Distillate is cooled down to 50 °C and liquid phase is recirculated to the column. Vapor phase enters the pressure swing adsorption (PSA) section where 280 kg/h of pure hydrogen is recovered. Recovered hydrogen is mixed with fresh purchased hydrogen and utilized for the catalytic upgrading.

2.5. Gas turbine (Brayton cycle), and utility (A600)

For heat and power generation this process design utilized Brayton power cycle or a stationary gas turbine (GT) (Figure S5). The GT was modeled according to the technical datasheet for the Siemens AG SGT-600 industrial gas turbine [51]. The GT features a maximum of

24.5 MW electrical power generation with gross efficiency of 33.6%, the pressure ratio of 14.0:1, and an exhaust temperature and a mass flow of 540 °C and 81.3 kg/s, respectively. The turbine was selected specifically as it has a proven use in combined heat and power plants, as well as its ability to utilize gaseous/liquid fuel mixtures. The GT housing was kept cooled at 150 °C operating temperature using a 56 ton/h of recirculating heat transfer fluid (terphenyl liquid); Therminol® 66 28, which has an upper operating temperature threshold of 345 °C. The hot heat transfer fluid was used to preheat wet seaweed before drying in section A100. The flue gasses from the GT exhaust supplied the main heat sinks of the process, pyrolysis, drying, and the column reboilers, as well as produced excess medium pressure steam to be sold as useful heat.

The main utilities (Figure S6) for this process are cooling water (inlet temperature = 28 °C; outlet temperature = 37 °C), medium pressure steam (171 °C; 7 bar), and electricity. The power produced in the GT is 10.4 MW of which the process consumes 60.3%. The total freshwater requirement is 56.6 ton/h of which the majority was for the cooling water requirement at 70%. The process produces 23 ton/h of medium pressure steam of which 70% is consumed in the column reboilers, while the rest is sold as useful heat.

3. Experiment-based simulation, and assessment methodology

Process simulation and design was based on experimental data related to the fast pyrolysis of *S. japonica* brown seaweed. The composition of this seaweed (Table S1) can be summarized as having a large volatile matter content (50–70 wt%) composed mostly of carbohydrates (positive aspect) and a significant mineral content (20–30 wt%) which is a negative aspect in terms of thermochemical processing. Experimental studies by Choi et al. [19] and Ly et al. [16] represent the empirical basis for the process design in this work. In their studies *S. japonica* macroalgae was subjected to fast pyrolysis in a bubbling fluidized bed reactor as depicted in Figure S16. [16]. In these studies, the fast pyrolysis conditions where the liquid product yield was maximized were optimized at varying temperatures, fluidization velocities, and pretreatment methods. As it can be observed from Fig. 3 the best temperature range was found to be between 375 °C and 400 °C yielding an average of 32.2 wt% of the liquid product (biocrude). The study has also demonstrated that using a non-intensive water wash pretreatment liquid reduces the mineral content of seaweeds from 31.5 wt% to 25.1 wt% and in turn increases the product yield from 18.3 wt% (non-treated seaweed at 375 °C) to 31.27 wt% (water-washed seaweed at 375 °C). For the proposed industrial scale system, pyrolysis conditions of 400 °C and 1.168 s of residence time were selected from the experimental studies as they yielded the most liquid product (31.04 wt%), which contained the largest amount of organic phase (48.98 wt%. of the liquid product). Separation of organic compounds from water in the biocrude (dewatering) via vacuum fractional distillation and upgrading of the dewatered biocrude via catalytic hydrogenation (100 bar, 350 °C, $CuCr_2O_3$ catalyst) was performed by Choi et al. [52,53] and was used as an empirical basis for upgraded biocrude fuel production.

The feedstock and main product mass balances from the fluidized bed fast pyrolysis experimental data can be summarized as follows. Water washed and dried seaweed is pyrolyzed at a temperature of 400 °C producing vaporized pyrolytic oil, light gasses, and solid residue (bio-char) with a mass yield product distribution of 31 wt%, 37 wt%, and 32 wt% respectively [19]. Furthermore, pyrolytic oil consists of lipophilic (organic phase) and hydrophilic (aqueous phase) organic compounds and water. The combined mass fraction of organic compounds in the pyrolytic oil is 56 wt%, while the rest is water [19]. The yield of upgraded biocrude fuel produced from seaweed-derived, dewatered biocrude by catalytic upgrading was 55 wt%. as determined by Choi [53]. Therefore, based on 1000 kg of dried *S. japonica* seaweed, 174 kg of biocrude (experimental composition described in Table 3) is produced by fast pyrolysis which in turn yields 95.7 kg of upgraded
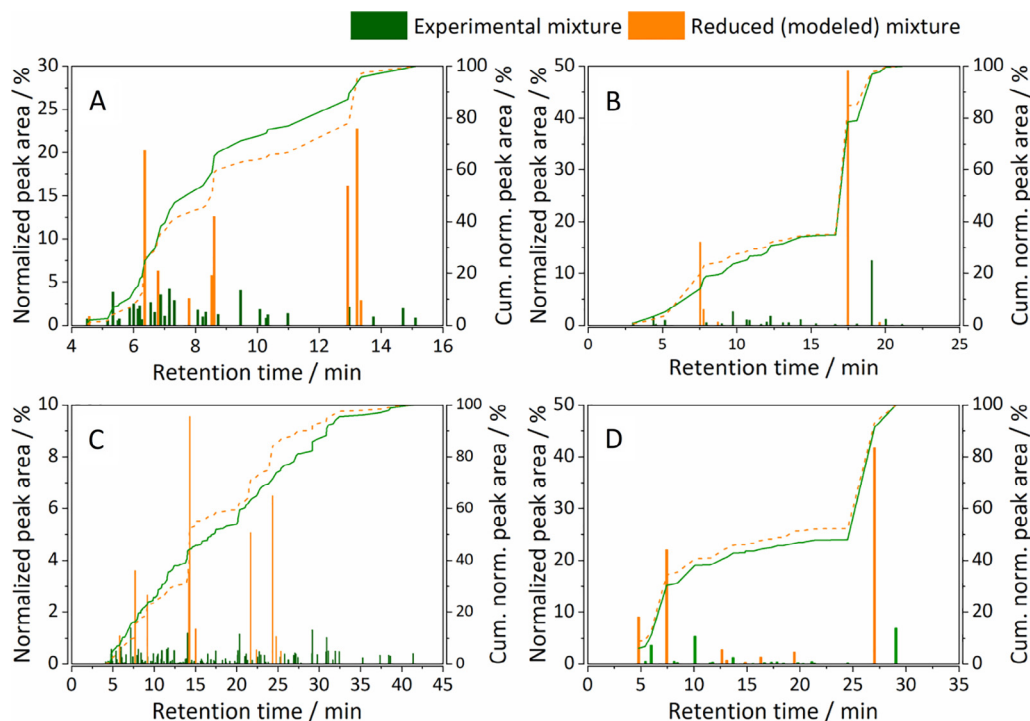
Fig. 4. Gas chromatogram with normalized and cumulative peak area of experimental and reduced (modeled) mixtures. Biocrude organic (A) and aqueous phase (B); Upgraded biocrude fuel organic (C) and aqueous (D) phase.

biocrude fuel.

3.1. Complex mixture modeling and process simulation

The proposed process was simulated, in steady-state, using Aspen Plus® V10 to obtain the material and energy balances. Biocrude and hydrocarbon fuel as complex organic mixtures, were modeled using a method developed by Brigljević et al. [47] where more detail is available of how this methodology is utilized to translate experimental data into a process simulation program. Utilizing GC–MS and elemental analysis data for seaweed biocrude from fluidized bed reactor system [19] and for hydrocarbon fuel produced from catalytic upgrading of seaweed biocrudes [53] optimal reduced mixtures were produced for simple yet accurate representation which can be time-efficiently handled by a process simulator (Fig. 4). The number of components in the reduced mixtures in comparison to the experimental ones was 64 to 15 and 161 to 23 for biocrude and hydrocarbon fuel, respectively. Find and replace function of the biocrude modelling method has been used to select structurally similar (in terms of boiling point, molecular mass and atomic composition) components which were not found in the process simulator's database. These compounds are outlined in Table 1 where CR and H represent crude and hydro-treated, respectively, as well as OR and AQ represent organic (lipophilic) and aqueous (hydrophilic), respectively.

3.2. Techno-economic assessment procedure

Estimation of the total capital investment (TCI) and minimum product selling price (MPSP) was the primary goal of the techno-economic assessment (TEA) in the scope of this work. The basis for the calculation of the TCI was the capital cost estimation of all the equipment for the current year and a summary of the material cost (e.g., raw materials, chemicals, and utilities). These estimates were used for the prediction of future earnings (cash flow trends), which were calculated using the following equation, as suggested by Dickson et al. [54]:

$$NCF_n = -r_n T_{CI} + a_n W_c + (\mathrm{Re}\,v - T_{COM})(1 - tax) + D \cdot tax \qquad (1)$$

where NCF_n is the non-discounted cash flow for the year n, r_n is the ratio of total capital investment consumed during year $\boldsymbol{n}$, $\boldsymbol{T_{CI}}$ is the sum of fixed capital investment and land cost, $\boldsymbol{T_{COM}}$ is the cost of manufacturing, $\boldsymbol{D}$ is depreciation, $\boldsymbol{Rev}$ is revenue, $\boldsymbol{tax}$ is the assumed tax rate and W_c is working capital. $\boldsymbol{a_n}$ is a parameter equal to -1 during year 3, 1 during the last year of the project, and zero for all other years. The net present value (NPV) was then calculated using the following equation:

$$NPV = \sum_{n=0}^{30} \frac{NCF_n}{(1 + r)^n} \qquad (2)$$

The MPSP of hydrocarbon fuel was determined when the value of NPV was set to reach zero during the total duration of the process by variation of the MPSP.

Prices of chemical engineering equipment not widely used, such as rotary vacuum filters or the industrial-scale CFB pyrolysis reactor, were sourced from either published works or directly from manufacturers. Costs of more established equipment, such as distillation columns, knock-out drums, decanters, pressure vessels, pumps, and compressors, were estimated using the Aspen Plus V10 Capital Cost Estimator. Literature obtained equipment costs were scaled to an appropriate capacity for the described process from the baseline costs using the following common equation:

$$C_n = C_{n,o} \left(\frac{Q_n}{Q_{n,o}} \right)^{a_n} \qquad (3)$$

where C_n is the new cost of the equipment, $C_{n,o}$ is the baseline cost, Q_n, and $Q_{n,o}$ are the capacity values (e.g., volume, flowrate, and power) for new equipment and baseline equipment, respectively, and a_n is the equipment type-dependent scaling exponent. All new equipment costs were adjusted for inflation to the year of analysis (2019) using the chemical engineering plant cost indices (CEPCI) and the following equation:

$$AC_n = C_n \left(\frac{CEPCI_{2019}}{CEPCI_{baseyear}} \right) \qquad (4)$$

Table 1
Biocrude and upgraded biocrude fuel model components and their structures as a result of the reduction software.

Component marking	Component name	Molecular formula	Structure
Biocrude model components			
CR-OR-1	Eicosene	$C_{20}H_{40}$	
CR-OR-2	Isoquinoline	C_9H_7N	
CR-OR-3	Indole	C_8H_7N	
CR-OR-4	Cyclohexyl methyl ketone	$C_8H_{14}O$	
CR-OR-5	Isopropyl ether	$C_6H_{14}O$	
CR-OR-6	Diethylaniline	$C_{10}H_{15}N$	
CR-OR-7	3,5-Dimethylpyridine	C_7H_9N	
CR-OR-8	2-Butene-1,4-diol	$C_4H_8O_2$	
CR-OR-9	Para-cresol	C_7H_8O	
CR-OR-10	Isosorbide	$C_6H_{10}O_4$	
CR-AQ-1	2,4-Hexadiene, 2,5-dimethyl-	C_8H_{14}	
CR-AQ-2	Heptanal	$C_7H_{14}O$	
CR-AQ-3	Cyclohexanone	$C_6H_{10}O$	
CR-AQ-4	5-Methyl-2-furaldehyde	$C_6H_6O_2$	
CR-AQ-5	Phenylhydrazine	$C_6H_8N_2$	
Upgraded biocrude fuel model components			
H-OR-1	Isobutylene	C_4H_8	
H-OR-2	Cis-2-pentene	C_5H_{10}	
H-OR-3	2,5-dimethyl-1,5-hexadiene	C_8H_{14}	
H-OR-4	2-hexanone	$C_6H_{12}O$	
H-OR-5	Toluene	C_7H_8	
H-OR-6	1-methyl-2-ethylbenzene	C_9H_{12}	
H-OR-7	1-(1-Tert-Butoxypropan-2-yloxy)propan-2-ol	$C_{10}H_{22}O_3$	
H-OR-8	Bicyclo-3–1-1-heptane	C_7H_{12}	
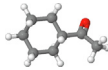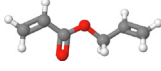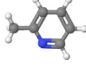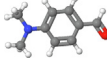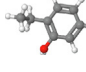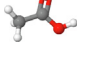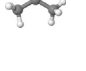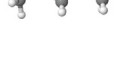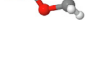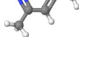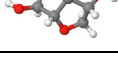
Table 1 (*continued*)

Component marking	Component name	Molecular formula	Structure
Biocrude model components			
H-OR-9	Cyclohexyl methyl ketone	$C_8H_{14}O$	
H-OR-10	Allyl-acrylate	$C_6H_8O_2$	
H-OR-11	2-methylpyridine	C_6H_7N	
H-OR-12	P-dimethylaminobenzaldehyde	$C_9H_{11}NO$	
H-OR-13	o-ethylphenol	$C_8H_{10}O$	
H-AQ-1	Acetic-acid	$C_2H_4O_2$	
H-AQ-2	Acetone	C_3H_6O	
H-AQ-3	2-hexanone	$C_6H_{12}O$	
H-AQ-4	Cyclohexanone	$C_6H_{10}O$	
H-AQ-5	Gamma-butyrolactone	$C_4H_6O_2$	
H-AQ-6	2-methylpyridine	C_6H_7N	
H-AQ-7	2,4,6-trimethylpyridine	$C_8H_{11}N$	
H-AQ-8	Isosorbide	$C_6H_{10}O_4$	

Table 2
Techno-economic assessment assumptions.

Term	Assumption
Equity	100%
Discount Rate (Internal Rate of Return [IRR])	10%
Income tax rate	25%
Total installed cost (TIC)	ISBL + Storage
Warehouse facility (*a*)	4% of TIC
Site development (*b*)	9% of TIC
Additional piping (*c*)	4.5% of TIC
Total direct cost (TDC)	TIC + a + b + c
Proratable expenses (*d*)	10% of TDC
Field expenses (*e*)	10% of TDC
Construction of the home office (*f*)	20% of TDC
Project contingency (*g*)	10% of TDC
Start-up and permits (*h*)	10% of TDC
Total indirect costs (TIDC)	d + e + f + g + h
Fixed capital investment (FCI)	TDC + TIDC
Land (*i*)	6% of TIC
Working capital (*j*)	5% of FCI
Total capital investment (TCI)	FCI + i + j
Labor and supervision (*k*)	1.6% of TCI
Maintenance (*l*)	3% of ISBL
Property insurance and property tax (*m*)	7% of TCI
Fixed operating costs (FOC)	k + l + m

where the adjusted equipment cost is AC_n, and $CEPCI_{2019}$ and $CEPCI_{base\ year}$ are the index values of the current year and year of the original equipment cost quote, respectively. with certain base assumptions outlined in Table 2. The total price of all the equipment or the inside battery limit (ISBL) was used as a base point for calculating TCI and fixed operating costs, together.

3.3. Sensitivity analysis, market uncertainty analysis, and environmental sustainability comparison with fossil fuel process

MPSP was subjected to sensitivity analysis using the predetermined variable factors and variation ranges in order to assess the degree of effect on the MPSP upon their variation. The parameters of the sensitivity analysis were divided into two groups, internal and external. Internal economic parameters consisted of fixed capital investment (FCI) working capital, income tax rate, and internal rate of return (IRR), whereas the external economic parameters (prices) were the prices of seaweed, olivine (heat carrier sand), power, and hydrogen. As these parameters vary through the process lifetime, so does the MPSP. To account for the market uncertainty, or the random values of sensitivity parameters during the project lifetime, MPSP price range was determined as a result of a Monte Carlo analysis. The end points of the price range were defined as the best- and worst-case MPSP scenarios. In other words when every sensitivity parameter of interest maximally reduced the MPSP was the best case and vice versa for the worst case. As it is highly unlikely that the price would reach that of the best or worst case at any time, the main question was in which range the price will most likely be in? 1,000 different scenarios of random values of sensitivity parameters (between predetermined variation ranges for each) generated 1000 different values of MPSP for which the normal

Table 3
Comparison of experimental and simulated biocrude and flowsheet simulation results outlining material, water, heat, and power production and utilization.

	Dewatered biocrude	
	Experimental	Modeled[a]
# of compounds	64	15
Comment	GC–MS detected	Modeled[a]
Mass yield; %	17.4	18.0
	Elemental composition	
C (wt. %)	69.29	71.06
H (wt. %)	7.69	9.39
N (wt. %)	6.10	14.27
O (wt. %)	13.39	5.28
HHV[b]; MJ/kg	31.21	34.29
Process outputs		
Main product stream	Unit	Value
Seaweed dry	ton/year	400,000
Dewatered biocrude	ton/year	69,306
Upgraded biocrude fuel	bbl./year	269,563
Water utilization		
Cooling water makeup	ton/h	38.9
Process and net heat		
Process steam water	ton/h	22.9
Process steam water makeup	ton/h	9.8
Process steam	ton/h	15.9
Net steam output	ton/h	6.9
Power production and output		
Gross power produced	MW	10.4
Net power	MW	4.1

[a] Using the biocrude modeling method by Brigljević et al. [47].
[b] HHV estimation model for pyrolytic oils by Demirbas et al. [55].

distribution was assumed. This was performed for five different values of NPV (0, 10, 35, 80, and 150 mil USD). The most probable selling price was assumed to be one standard deviation from the mean price at a given value of NPV.

The carbon footprint of the proposed process encompassing harvesting, delivery and biofuel production was compared with that of an equivalent (sea platform) crude oil extraction, delivery, and refining process based on the total CO_2 emissions per kilogram of feedstock material. The purpose of this simplistic comparison (as opposed to a more comprehensive one such as life cycle assessment) was to give a general quantifiable indication of the proposed biorefinery's environmental sustainability.

4. Results and discussion

4.1. Mixture modeling and process simulation results

A comprehensive steady-state simulation model (Figure S7-S15) of the fluidized-bed fast-pyrolysis cogeneration was built using Aspen Plus V10. The main flowsheet consisted of seven hierarchical blocks composed the main flowsheet (Figure S7), where each one contained a process area governed by a primary property method and stream class for that area.

On the scale of 400,000 dry tons of seaweed per year (Table 3), the biorefinery produces 69.3 thousand tons of dewatered biocrude per year, and outputs 270 thousand bbl. of upgraded biocrude fuel per year as the main product. Main consumer of cooling water was the phase separation section with 92% of the total cooling water requirement by the process, predominately due to the distillation tower condenser. The rest of the cooling requirement is utilized by the product recovery distillation column. The total water consumption for the process steam generation was 22.9 ton/h with 43% being the makeup water. Net steam generated as a product was 6.9 ton/h. Of the total gross power produced in the process (Table 3) 10.4 MW, 4.1 MW was sold to the grid. Fig. 5B demonstrates the power consumption breakdown by process area. The pretreatment section consumed the most electricity (44%) due to the power intensive operations of physical feedstock handling (grinding, mixing, filtering, conveying, etc.), and since it handles a large amount of material by volume, as seaweed enters the process with 85 wt% of water content. Compressors for fluidizing gas and pyrolysis products, as well as the hot sand conveyors predominately contribute to the second most energy intensive area (A200) with 26%. Recovery and PSA were the third most energy intensive area contributing 13% of the total electricity consumption, predominately due to the high pressure required for the catalytic hydrogenation (100 bar).

4.2. Capital investment, manufacturing cost, and minimum product selling price determination

The total capital investment was determined at 170 million USD (Table 4). The primary capital cost contributors (Fig. 5A) in terms percentages of the total installed cost (TIC) were product upgrading and recovery (31% of the TIC), pyrolysis (29% of the TIC), and the gas turbine (24% of the TIC). Since the product upgrading requires significant temperature, and pressure conditions (100 bar, 300 °C) the cost
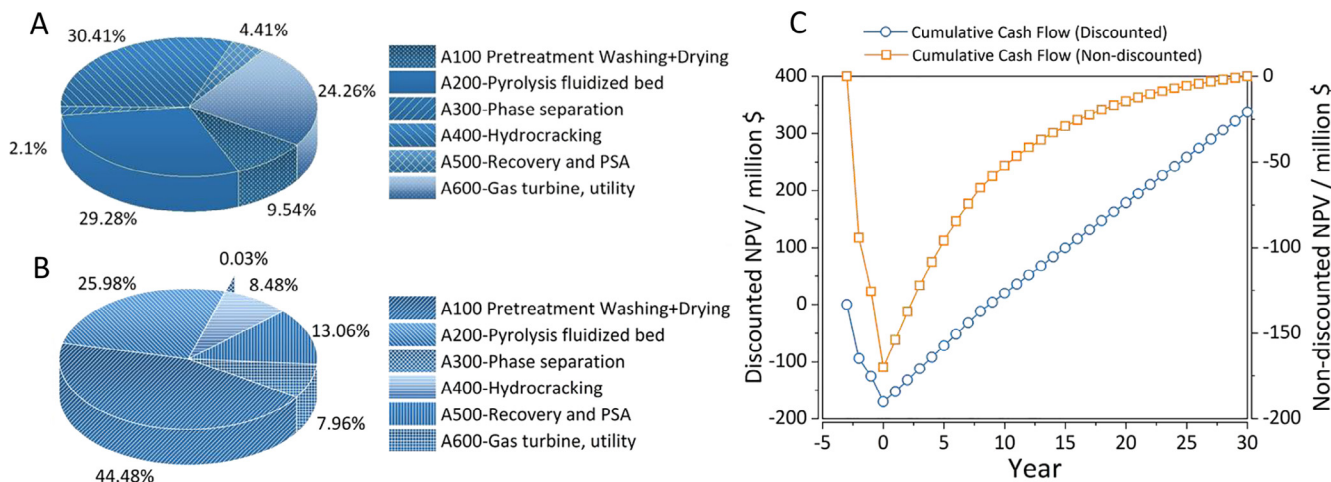

Fig. 5. Breakdown by process section of the total installed cost (A) and power consumption (B). Non-discounted and discounted cumulative cash flows (C) considering a 3-year construction and start-up period and 30 years of project life.

Table 4
Capital investment and manufacturing costs.

Capital investment costs			
Cost category		[million USD (2019)]	
Inside battery limit (ISBL)		82.1	
Total installed cost (TIC)		83.6	
Total direct costs (TDC)		98.2	
Total indirect costs (TIDC)		58.9	
Fixed capital investment (FCI)		157.1	
Fixed operating costs (FOC)		17.1	
Total capital investment (TCI)		170	
Costs of Manufacturing			
Raw materials and chemicals	Flowrate	Flowrate Unit	Price (2019 USD/Unit h)
Seaweed dry basis	50,000	kg/h	0.068
Olivine sand (fine) makeup	500	kg/h	0.19
Hydrocracking catalyst	0.0452	kg/h	58.32
Freshwater for washing	6,806	kg/h	6.70E-05
Cooling tower chemicals	0.4481	kg/h	1.12
Boiler feed water chemicals	0.3263	kg/h	0.68
Net Hydrogen (pipeline)	262	kg/h	4.5
Utilities			
Cooling water makeup	40,000	kg/h	6.70E-05
Steam gen water makeup	9,792	kg/h	6.70E-05
Waste streams			
Brine	306	ton/hr	0.008
Ash	12,047	kg/h	0.02
Flue gas (CO2 eqv.)	61.3	ton/h	
Flue gas (CO2 eqv.) including fixation	1.3	ton/h	20
Products			
Net Power produced	4,125	kW	0.102
Steam/MP	6,892	kg/h	0.011
Upgraded biocrude fuel	4,050	kg/h	varies

of materials for the section was expectedly high. Industrial scale circulating fluidized bed pyrolyzer is a rather novel concept which was also reflected in the price of this unit. The cost of the gas turbine required for this process was evaluated according to an assessment by Breeze [56] where for systems of similar scale the price was estimated at 917 USD/kW of total electrical power output rating of the gas turbine.

Annual manufacturing costs for the process are presented in Table 4 where the average price of the feedstock material was assumed at 68 USD per dry ton and purchase price of pipeline-delivered hydrogen was averaged at 4.5 USD per kg. The main waste streams of the process were brine water and fly ash from combustion, for which the cost of treatment and disposal were accounted for at 0.77 USD per ton and 20 USD per ton, respectively. The process design considered the use of an outside contractor for wastewater treatment, and a carbon tax for the total CO_2 equivalent in the flue gasses. The greatest contributors to the total annual cost the seaweed and fixed operating costs having 42.8% and 38% share respectfully. Other raw materials and chemicals, utilities, and cost of waste disposal contributed 16%, 0.04%, and 3% respectively.

Non-discounted and discounted cumulative cash flows (Fig. 5C) were determined for considering a 3-year construction and start-up period and 30 years of project life. Non-discounted cumulative cash flow achieved zero value at the end of project life as the minimum upgraded biocrude selling price was reached at 1.6941 USD/L (6.41 USD/gal; 269.34 USD/bbl). Compared purely on the selling price the MPSP is 1.6 times higher than the current global average of fossil fuel produced upgraded biocrude (1.03 USD/L [57]). This of course entails that the price difference is most likely even higher for a profit generating biorefinery even after considering the market fluctuations of crude oil derivates.

4.3. Process market sensitivity and the resulting selling price ranges

One-point sensitivity analysis was performed on the total of eight parameters. As it can be observed from Fig. 6A the MPSP was the most sensitive to the change in FCIL and IRR in terms of internal economic parameters. In terms of external parameters seaweed purchase price had the most effect followed by the price of olivine sand and hydrogen price. Monte Carlo (market uncertainty) analysis was performed on MPSP and on product selling prices of four additional values of NPV 10, 35, 80, and 100 million USD. 1000 prices as a result of cumulative effect of random sensitivity parameter values for each NPV case were generated. Assuming normal distribution from the average price within each NPV case, price ranges were estimated as evident from the box and whiskers plots depicted in Fig. 6B. As NPV of the process moves from 0 to 150 million USD the most probable selling price ranges shit from 1.534 to 1.852 USD/L to 1.952–2.346 USD/L. This is analogous to the changes in values of returns on investments as they shift from 8.7 and 30 years (at NPV = 0 mil. USD) to 4.6 and 6.6 (at NPV = 150 mil. USD) for discounted and non-discounted ROIs respectively.

4.4. Environmental sustainability comparison with crude oil

The process was compared with traditional oil and gas production based on the total CO_2 or CO_2 eqv. emissions per unit mass of processed crude oil and per unit mass of dry seaweed. CO_2 emissions from oil extraction operations, delivery, and processing were conservatively averaged (in favor of less emissions from crude oil process) at 0.32 kg of CO_2 emitted per kg of crude oil and used as a point of comparison [58,59]. Using flowsheet simulation results emission of 1.226 kg of CO_2 per kg of dry seaweed processed was calculated. The total CO_2 emissions from seaweed harvesting and transport of 0.19 kg per kg dry wt. were determined from an LCA study by Alvarado-Morales et al. [60]. This was calculated from the total resources used for harvesting and transport of 1000 kg of dry seaweed, which are reported to be 30 L of petrol, 30 L of upgraded biocrude, and 30 kWh of grid electricity. The assumed emissions for petrol, upgraded biocrude, and grid electricity were 2.31 kg/L, 2.68 kg/L, and 1.183 kg/kWh (where the worst case of a coal power plant was assumed), respectively. Furthermore, CO_2 emission variation (due to possible disparate and unstandardized supply chains) was considered assuming an emission bad case scenario of 0.5 kg of CO_2 per kg of dry seaweed. Finally, an average of 1.7 kg of CO_2 per kg of dry seaweed from large-scale seaweed farming was taken into account as the amount of fixed CO_2 [61]. Therefore, the final estimated emission value for the process was 0.025 kg of CO_2 per kg of dry seaweed (Fig. 6C). This reveals the significant and beneficial environmental potential (in addition to the inherent sustainability of the biofuel platform) of this process as the CO_2 emissions are reduced by ~ 13-fold when compared with conventional crude oil processing.

5. Conclusions and observations

For the first time, a comprehensive, experiment-based process design and assessment of a seaweed biofuel, heat and power production process featuring an integration of a Bryton power cycle with an industrial scale circulating bed pyrolysis was presented. The complex organic mixtures are modeled with a specialized software using experimental data for two key chemical conversions: pyrolysis and catalytic upgrading, which ensured a realistic process simulation.

Although the determined minimum selling price range of 1.534–1.852 USD/L is considerably higher than the global average price of crude oil derived diesel fuel, the proposed seaweed biofuel production process exhibits a significant ~ 13-fold reduction of CO_2 emission compared to conventional crude oil refining.

This leads to the conclusion that even though fuels from seaweed based biorefineries might still be twice as expensive as fuels from traditional crude oil processes, process designs that feature strategic
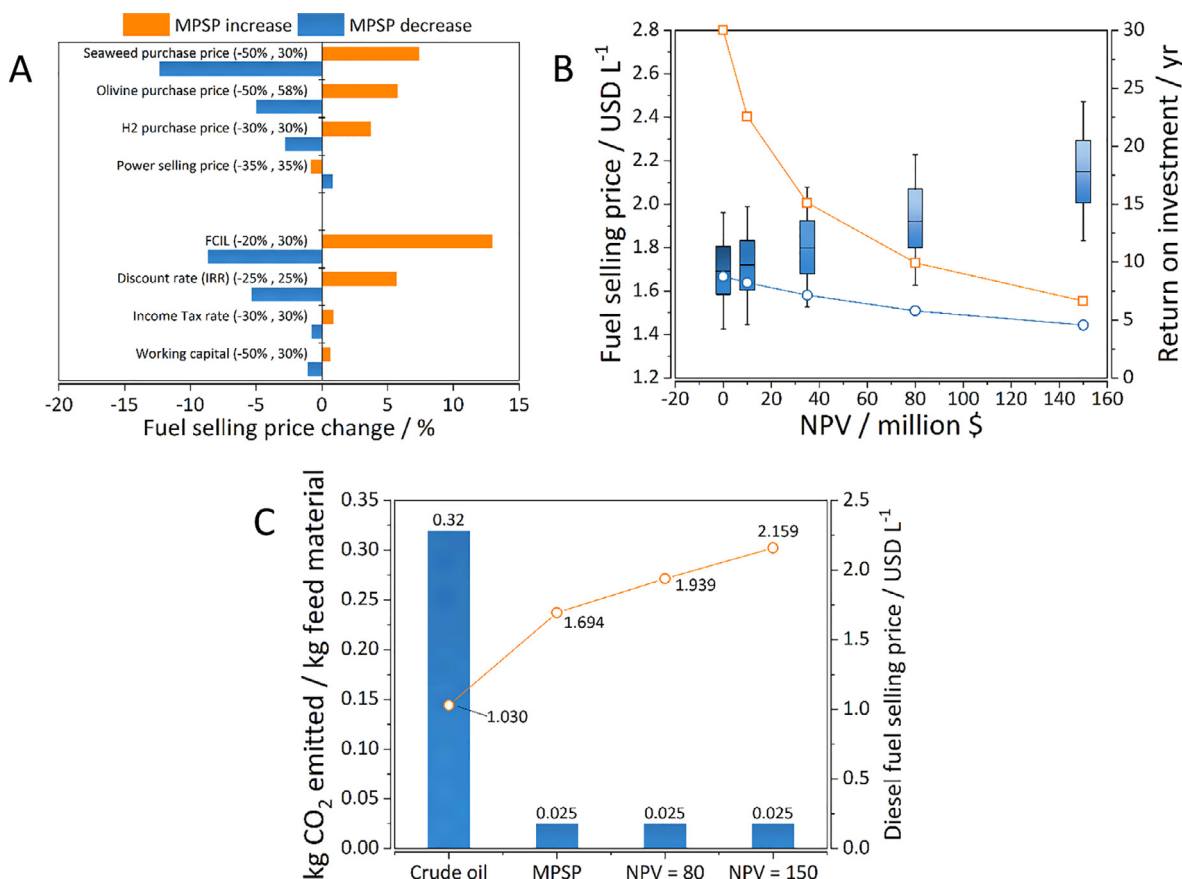
Fig. 6. One-point sensitivity analysis of external (UP) and internal (DOWN) economic parameters (A). Return on investment (line and marker) and product selling price ranges (box and whiskers) at different values of NPV. Square and round markers stand for non-discounted and discounted ROI respectively (B). Carbon emission and upgraded biocrude fuel selling price comparison from traditional crude oil process and seaweed fast pyrolysis process (C).

integration of conversion technologies have the potential to even the playfield from the ground up. Furthermore, as the conversion technologies progress as well as feedstock supply chains become more predictable so will the process economics improve significantly. As a final note, it is of vital importance to quantify the beneficial environmental effects of utilizing this feedstock on a large scale, if not just for the justification of the price difference, but also to point out the inherent unsustainability of our global fossil fuel demand.

Declaration of Competing Interest

None

Acknowledgements

Appendix A. Supplementary data

Supplementary data to this article can be found online at https://doi.org/10.1016/j.enconman.2019.05.103.

References

[1] Giampietro M, Mayumi K. The biofuel delusion: The fallacy of large scale agro-biofuels production. Sterling, VA: Earthscan London; 2009.

[2] Özdenkçi K, De Blasio C, Muddassar HR, Melin K, Oinas P, Koskinen J, et al. A novel biorefinery integration concept for lignocellulosic biomass. Energy Convers Manag 2017;149:974–87. https://doi.org/10.1016/j.enconman.2017.04.034.

[3] Uzoejinwa BB, He X, Wang S, El-Fatah Abomohra A, Hu Y, Wang Q. Co-pyrolysis of biomass and waste plastics as a thermochemical conversion technology for high-grade biofuel production: recent progress and future directions elsewhere worldwide. Energy Convers Manag 2018;163:468–92. https://doi.org/10.1016/j.enconman.2018.02.004.

[4] Jang BW, Gläser R, Liu C, Capel-sanchez MC, Campos-martin JM, Fierro LG, et al. Fuels of the future. Energy Environ Sci 2010;3:253. https://doi.org/10.1039/c003390c.

[5] Cole A, Dinburg Y, Haynes BS, He Y, Herskowitz M, Jazrawi C, et al. From macroalgae to liquid fuel via waste-water remediation, hydrothermal upgrading, carbon dioxide hydrogenation and hydrotreating. Energy Environ Sci 2016;9:1828–40. https://doi.org/10.1039/C6EE00414H.

[6] Chen WT, Zhang Y, Zhang J, Schideman L, Yu G, Zhang P, et al. Co-liquefaction of swine manure and mixed-culture algal biomass from a wastewater treatment system to produce bio-crude oil. Appl Energy 2014;128:209–16. https://doi.org/10.1016/j.apenergy.2014.04.068.

[7] Gao K, McKinley KR. Use of macroalgae for marine biomass production and CO2 remediation: a review. J Appl Phycol 1994;6:45–60. https://doi.org/10.1007/BF02185904.

[8] Adams JMM, Ross AB, Anastasakis K, Hodgson EM, Gallagher JA, Jones JM, et al. Seasonal variation in the chemical composition of the bioenergy feedstock Laminaria digitata for thermochemical conversion. Bioresour Technol 2011;102:226–34. https://doi.org/10.1016/j.biortech.2010.06.152.

[9] Wei N, Quarterman J, Jin YS. Marine macroalgae: An untapped resource for producing fuels and chemicals. Trends Biotechnol 2013;31:70–7. https://doi.org/10.1016/j.tibtech.2012.10.009.

[10] Roesijadi G, Jones SB, Snowden-Swan LJ, Zhu Y. Macroalgae as a biomass feedstock: a preliminary analysis, PNNL 19944. Richland: 2010.

[11] Jensen A. Present and future needs for algae and algal products. Hydrobiologia 1993;260–261:15–23. https://doi.org/10.1007/BF00048998.

[12] Ross A, Jones J, Kubacki M, Bridgeman T. Classification of macroalgae as fuel and its thermochemical behaviour. Bioresour Technol 2008;99:6494–504. https://doi.org/10.1016/j.biortech.2007.11.036.

[13] Duarte CM, Middelburg JJ, Caraco N. Major role of marine vegetation on the oceanic carbon cycle. Biogeosciences 2005;2:1–8. https://doi.org/10.5194/bg-2-1-2005.

[14] Ross AB, Anastasakis K, Kubacki M, Jones JM. Investigation of the pyrolysis behaviour of brown algae before and after pre-treatment using PY-GC/MS and TGA. J Anal Appl Pyrolysis 2009;85:3–10. https://doi.org/10.1016/j.jaap.2008.11.004.

[15] Choi JH, Kim SS, Ly HV, Kim J, Woo HC. Thermogravimetric characteristics and pyrolysis kinetics of high-density-aquacultured Saccharina Japonica: Effects of water-washing. Fuel 2017;193:159–67. https://doi.org/10.1016/j.fuel.2016.12.041.

[16] Ly HV, Kim SS, Woo HC, Choi JH, Suh DJ, Kim J. Fast pyrolysis of macroalga Saccharina japonica in a bubbling fluidized-bed reactor for bio-oil production. Energy 2015;93:1436–46. https://doi.org/10.1016/j.energy.2015.10.011.

[17] Ly HV, Kim SS, Choi JH, Woo HC, Kim J. Fast pyrolysis of Saccharina japonica alga in a fixed-bed reactor for bio-oil production. Energy Convers Manag 2016;122:526–34. https://doi.org/10.1016/j.enconman.2016.06.019.

[18] Li D, Chen L, Yi X, Zhang X, Ye N. Pyrolytic characteristics and kinetics of two brown algae and sodium alginate. Bioresour Technol 2010;101:7131–6. https://doi.org/10.1016/j.biortech.2010.03.145.

[19] Choi JH, Kim SS, Ly HV, Kim J, Woo HC. Effects of water-washing Saccharina japonica on fast pyrolysis in a bubbling fluidized-bed reactor. Biomass Bioenergy 2017;98:112–23. https://doi.org/10.1016/j.biombioe.2017.01.006.

[20] Choi JH, Kim SS, Suh DJ, Jang EJ, Il Min K, Woo HC. Characterization of the bio-oil and bio-char produced by fixed bed pyrolysis of the brown alga Saccharina japonica. Korean J Chem Eng 2016;33:2691–8. https://doi.org/10.1007/s11814-016-0131-5.

[21] Chen D, Mei J, Li H, Li Y, Lu M, Ma T, et al. Combined pretreatment with torrefaction and washing using torrefaction liquid products to yield upgraded biomass and pyrolysis products. Bioresour Technol 2017;228:62–8. https://doi.org/10.1016/j.biortech.2016.12.088.

[22] Chen D, Cen K, Jing X, Gao J, Li C, Ma Z. An approach for upgrading biomass and pyrolysis product quality using a combination of aqueous phase bio-oil washing and torrefaction pretreatment. Bioresour Technol 2017;233:150–8. https://doi.org/10.1016/j.biortech.2017.02.120.

[23] Cen K, Zhang J, Ma Z, Chen D, Zhou J, Ma H. Investigation of the relevance between biomass pyrolysis polygeneration and washing pretreatment under different severities: water, dilute acid solution and aqueous phase bio-oil. Bioresour Technol 2019;278:26–33. https://doi.org/10.1016/j.biortech.2019.01.048.

[24] Moncada J, El-Halwagi MM, Cardona CA. Techno-economic analysis for a sugarcane biorefinery: Colombian case. Bioresour Technol 2013;135:533–43. https://doi.org/10.1016/j.biortech.2012.08.137.

[25] Gnansounou E, Vaskan P, Pachón ER. Comparative techno-economic assessment and LCA of selected integrated sugarcane-based biorefineries. Bioresour Technol 2015;196:364–75. https://doi.org/10.1016/j.biortech.2015.07.072.

[26] Huang H, Long S, Singh V. Techno-economic analysis of biodiesel and ethanol co-production from lipid-producing sugarcane. Biofuels, Bioprod Biorefining n.d.;10:299–315. doi:10.1002/bbb.1640.

[27] Kazi FK, Fortman JA, Anex RP, Hsu DD, Aden A, Dutta A, et al. Techno-economic comparison of process technologies for biochemical ethanol production from corn stover. Fuel 2010;89:S20–8. https://doi.org/10.1016/j.fuel.2010.01.001.

[28] Tao L, He X, Tan ECD, Zhang M, Aden A. Comparative techno-economic analysis and reviews of n-butanol production from corn grain and corn stover. Biofuels Bioprod Biorefining n.d.;8:342–61. doi:10.1002/bbb.1462.

[29] Klein-Marcuschamer D, Simmons BA, Blanch HW. Techno-economic analysis of a lignocellulosic ethanol biorefinery with ionic liquid pre-treatment. Biofuels Bioprod Biorefining n.d.;5:562–9. doi:10.1002/bbb.303.

[30] Sassner P, Galbe M, Zacchi G. Techno-economic evaluation of bioethanol production from three different lignocellulosic materials. Biomass Bioenergy 2008;32:422–30. https://doi.org/10.1016/j.biombioe.2007.10.014.

[31] Patel M, Zhang X, Kumar A. Techno-economic and life cycle assessment on lignocellulosic biomass thermochemical conversion technologies: a review. Renew Sustain Energy Rev 2016;53:1486–9. https://doi.org/10.1016/j.rser.2015.09.070.

[32] Hamelinck CN, Van Hooijdonk G, Faaij APC. Ethanol from lignocellulosic biomass: techno-economic performance in short-, middle- and long-term. Biomass Bioenergy 2005;28:384–410. https://doi.org/10.1016/j.biombioe.2004.09.002.

[33] Piccolo C, Bezzo F. A techno-economic comparison between two technologies for bioethanol production from lignocellulose. Biomass Bioenergy 2009;33:478–91. https://doi.org/10.1016/j.biombioe.2008.08.008.

[34] Wright MM, Satrio JA, Brown RC, Daugaard DE, Hsu DD. Techno-economic analysis of biomass fast pyrolysis to transportation fuels. Natl Renew Energy Lab 2010;89:S2–10. https://doi.org/10.1016/j.fuel.2010.07.029.

[35] Zamalloa C, Vulsteke E, Albrecht J, Verstraete W. The techno-economic potential of renewable energy through the anaerobic digestion of microalgae. Bioresour Technol 2011;102:1149–58. https://doi.org/10.1016/j.biortech.2010.09.017.

[36] Davis R, Aden A, Pienkos PT. Techno-economic analysis of autotrophic microalgae for fuel production. Appl Energy 2011;88:3524–31. https://doi.org/10.1016/j.apenergy.2011.04.018.

[37] Nagarajan S, Chou SK, Cao S, Wu C, Zhou Z. An updated comprehensive techno-economic analysis of algae biodiesel. Bioresour Technol 2013;145:150–6. https://doi.org/10.1016/j.biortech.2012.11.108.

[38] Beal CM, Gerber LN, Sills DL, Huntley ME, Machesky SC, Walsh MJ, et al. Algal biofuel production for fuels and feed in a 100-ha facility: A comprehensive techno-economic analysis and life cycle assessment. Algal Res 2015;10:266–79. https://doi.org/10.1016/j.algal.2015.04.017.

[39] Quinn JC, Davis R. The potentials and challenges of algae based biofuels: a review of the techno-economic, life cycle, and resource assessment modeling. Bioresour Technol 2015;184:444–52. https://doi.org/10.1016/j.biortech.2014.10.075.

[40] Koutinas AA, Chatzifragkou A, Kopsahelis N, Papanikolaou S, Kookos IK. Design and techno-economic evaluation of microbial oil production as a renewable resource for biodiesel and oleochemical production. Fuel 2014;116:566–77. https://doi.org/10.1016/j.fuel.2013.08.045.

[41] Kaur M, Srikanth S, Kumar M, Sachdeva S, Puri SK. An integrated approach for efficient conversion of Lemna minor to biogas. Energy Convers Manag 2019;180:25–35. https://doi.org/10.1016/j.enconman.2018.10.106.

[42] Fasahati P, Liu JJ. Impact of volatile fatty acid recovery on economics of ethanol production from brown algae via mixed alcohol synthesis. Chem Eng Res Des 2015;98:107–22. https://doi.org/10.1016/j.cherd.2015.04.013.

[43] Fasahati P, Saffron CM, Woo HC, Liu JJ. Potential of brown algae for sustainable electricity production through anaerobic digestion. Energy Convers Manag 2017;135:297–307. https://doi.org/10.1016/j.enconman.2016.12.084.

[44] Fasahati P, Liu JJ. Application of MixAlco® processes for mixed alcohol production from brown algae: economic, energy, and carbon footprint assessments. Fuel Process Technol 2016;144:262–73. https://doi.org/10.1016/j.fuproc.2016.01.008.

[45] Jones S, Meyer P, Snowden-Swan L, Susanne KJ, Pimphan M, Snowden-SwanLesley, et al. Process design and economics for the conversion of lignocellulosic biomass to hydrocarbon fuels: Fast pyrolysis and hydrotreating bio-oil pathway. US Dep Energy 2013:97. doi:PNNL - 23053 NREL/TP - 5100 - 61178.

[46] Jones SB, Holladay JE, Valkenburg C, Stevens DJ, Walton CW, Kinchin C. Production of Gasoline and Diesel from Biomass via Fast Pyrolysis. Hydrotreating and Hydrocracking A Design Case 2009.

[47] Brigljević B, Žuvela P, Liu JJ, Woo HC, Choi JH. Development of an automated method for modelling of bio-crudes originating from biofuel production processes based on thermochemical conversion. Appl Energy 2018;215:670–8. https://doi.org/10.1016/j.apenergy.2018.02.030.

[48] Van Nguyen T, Clausen LR. Techno-economic analysis of polygeneration systems based on catalytic hydropyrolysis for the production of bio-oil and fuels. Energy Convers Manag 2019;184:539–58. https://doi.org/10.1016/j.enconman.2019.01.070.

[49] Zhang X, Liu X, Sun X, Jiang C, Li H, Song Q, et al. Thermodynamic and economic assessment of a novel CCHP integrated system taking biomass, natural gas and geothermal energy as co-feeds. Energy Convers Manag 2018;172:105–18. https://doi.org/10.1016/j.enconman.2018.07.002.

[50] Dutta A, Sahir A, Tan E, Humbird D, Snowden-Swan LJ, Meyer P, et al. Process Design and Economics for the Conversion of Lignocellulosic Biomass to Hydrocarbon Fuels. Thermochemical Research Pathways with In Situ and Ex Situ Upgrading of Fast Pyrolysis Vapors Pacific Northwest National Lab. (PNNL), Richland, WA (United States) 2015. https://doi.org/10.2172/1215007.

[51] Siemens AG. Power-and-Gas-Division Distributed-Generation. Gas turbine SGT-600 For power generation and mechanical drive applications. Siemens AG SGT-600 Factsheet 2016.

[52] Choi JH, Kim S-S, Woo HC. Characteristics of vacuum fractional distillation from pyrolytic macroalgae (Saccharina japonica) bio-oil. J Ind Eng Chem 2017;51:206–15. https://doi.org/10.1016/j.jiec.2017.03.002.

[53] Choi JH. Pyrolysis and Catalytic Upgrading of Microalgal Biomass for Liquid Biofuel Production. Pukyong National University, 2015.

[54] Dickson R, Ryu J-H, Liu JJ. Optimal plant design for integrated biorefinery producing bioethanol and protein from Saccharina japonica: a superstructure-based approach. Energy 2018. https://doi.org/10.1016/j.energy.2018.09.007.

[55] Demirbas A, Gullu D, Çaglar A, Akdeniz F. Estimation of Calorific Values of Fuels from Lignocellulosics. Energy Sources 1997;19:765–70. https://doi.org/10.1080/00908319708908888.

[56] Breeze P. The Cost of Power Generation. Bus Insight 2010:147.

[57] GlobalPetrolPrices.com. https://www.globalpetrolprices.com/diesel_prices/; 10.09.2018 n.d. https://www.globalpetrolprices.com/diesel_prices/ (accessed February 8, 2019).

[58] Kwasniewski V, Blieszner J, Nelson R. Petroleum refinery greenhouse gas emission variations related to higher ethanol blends at different gasoline octane rating and pool volume levels. Biofuels Bioprod Biorefining n.d.;10:36–46. doi:10.1002/bbb.1612.

[59] Gavenas E, Rosendahl KE, Skjerpen T. CO2-emissions from Norwegian oil and gas extraction. Energy 2015;90:1956–66. https://doi.org/10.1016/j.energy.2015.07.025.

[60] Alvarado-Morales M, Boldrin A, Karakashev DB, Holdt SL, Angelidaki I, Astrup T. Life cycle assessment of biofuel production from brown seaweed in Nordic conditions. Bioresour Technol 2013;129:92–9. https://doi.org/10.1016/j.biortech.2012.11.029.

[61] Singh SP, Singh P. Effect of CO2 concentration on algal growth: a review. Renew Sustain Energy Rev 2014;38:172–9. https://doi.org/10.1016/j.rser.2014.05.043.